Ghostly tributaries to the Milky Way: charting the halo's stellar streams with the Gaia DR2 catalogue

Khyati Malhan, Rodrigo Ibata, Nicolas Martin

Monthly Notices
of the
ROYAL ASTRONOMICAL SOCIETY

MNRAS **481,** 3442–3455 (2018)
Advance Access publication 2018 September 11

doi:10.1093/mnras/sty2474

Ghostly tributaries to the Milky Way: charting the halo's stellar streams with the Gaia DR2 catalogue

Khyati Malhan,[1]★ Rodrigo A. Ibata[1] and Nicolas F. Martin[1,2]

[1]*Observatoire Astronomique de Strasbourg, Université de Strasbourg, CNRS, UMR 7550, F-67000 Strasbourg, France*
[2]*Max-Planck-Institut für Astronomie, Königstuhl 17, D-69117 Heidelberg, Germany*

Accepted 2018 September 5. Received 2018 August 11; in original form 2018 May 1

ABSTRACT

We present a panoramic map of the stellar streams of the Milky Way based upon astrometric and photometric measurements from the Gaia DR2 catalogue. In this first contribution, we concentrate on the halo at heliocentric distances beyond 5 kpc, and at Galactic latitudes $|b| > 30^\circ$, using the STREAMFINDER algorithm to detect structures along plausible orbits that are consistent with the Gaia proper motion measurements. We find a rich network of criss-crossing streams in the halo. Some of these structures were previously known, while several are new discoveries, but others are potentially artefacts of the Gaia scanning law and will require confirmation. With these initial discoveries, we are starting to unravel the complex formation of the halo of our Galaxy.

Key words: stars: kinematics and dynamics – Galaxy: halo – Galaxy: kinematics and dynamics – Galaxy: structure.

1 INTRODUCTION

The central position that stellar streams hold for Galactic archeology studies motivates conducting a thorough census of such structures in the Milky Way. Besides testing the hierarchical merging scenario of Galaxy formation (Johnston, Hernquist & Bolte 1996; Helmi & White 1999), the number of stellar streams can, in principle, be used to put a lower limit on past accretion events into the Galactic halo; their orbital structures can be used to probe the mass distribution and shape of the Milky Way dark matter halo (Johnston et al. 1999; Ibata et al. 2001; Eyre & Binney 2009; Koposov, Rix & Hogg 2010; Law & Majewski 2010; Küpper et al. 2015; Bovy et al. 2016); stream gaps can provide indirect evidence for the existence of dark matter sub-haloes (Johnston, Spergel & Haydn 2002; Carlberg, Grillmair & Hetherington 2012; Erkal et al. 2016; Sanders, Bovy & Erkal 2016); these structures can also be used to constrain the models of the formation and evolution of globular clusters (Balbinot & Gieles 2018). Furthermore, analyses based on the quantity and the collective phase-space distribution of stellar streams hold great promise in addressing some small-scale ΛCDM problems (such as the 'missing satellite problem' and the 'plane-of-satellites' problem, see e.g. Bullock and Boylan-Kolchin 2017).

Such considerations have motivated many previous studies to detect and analyse stellar streams in our Galaxy. Notable efforts in the past include the 'field-of-streams' map (Belokurov et al. 2006) of the region around the North Galactic Cap based on the SDSS DR5, which was expanded to cover both the Northern and Southern Galactic Cap regions in later SDSS releases (see e.g. Grillmair & Carlin 2016): Bernard et al. (2014) created a panoramic map of the entire Milky Way halo north of $\delta \sim -30^\circ$ ($\sim$30 000 deg^2) based on the Pan-STARRS1 data set; Mateu, Read, and Kawata (2018) applied a pole-counts stream-finding method to the Catalina RR-Lyrae survey revealing 14 candidate streams in the inner Galaxy; most recently Shipp et al. (2018) discovered 11 stellar streams out to a distance of $d_\odot \sim 50$ kpc by making use of the data from the Dark Energy survey (DES). The regions of sky covered by presently-known streams have been conveniently compiled in the GALSTREAMS python package (Mateu et al. 2018), which we reproduce in Fig. 1 for comparison to our results.

Given the arrival of all-sky data of unprecedented astrometric quality from the ESA/Gaia survey (de Bruijne 2012; Gaia Collaboration 2016), we built a stream-finding algorithm (the STREAMFINDER, Malhan and Ibata 2018, hereafter Paper I) to make use of the kinematic information that Gaia provides. The idea that we incorporated in the STREAMFINDER algorithm is that stellar streams can be found more efficiently by searching along possible orbital trajectories in the underlying gravitational potential of the Galaxy. In Paper I, our tests, based on a suite of *N*-body simulations embedded in a mock Galactic survey, showed that the algorithm is able to detect distant halo stream structures containing as few as $\sim$15 members (or equivalent with a surface brightness as low as $\Sigma_G \sim 33.6$ mag arcsec^{-2}) in the end-of-mission Gaia data set. The detection limit depends on various factors, such as the stream structure itself and its location in phase space with respect to the contaminating background. For instance, in Ibata et al. (2018) we reported the discovery of the (high con-

★ E-mail: kmalhan07@gmail.com

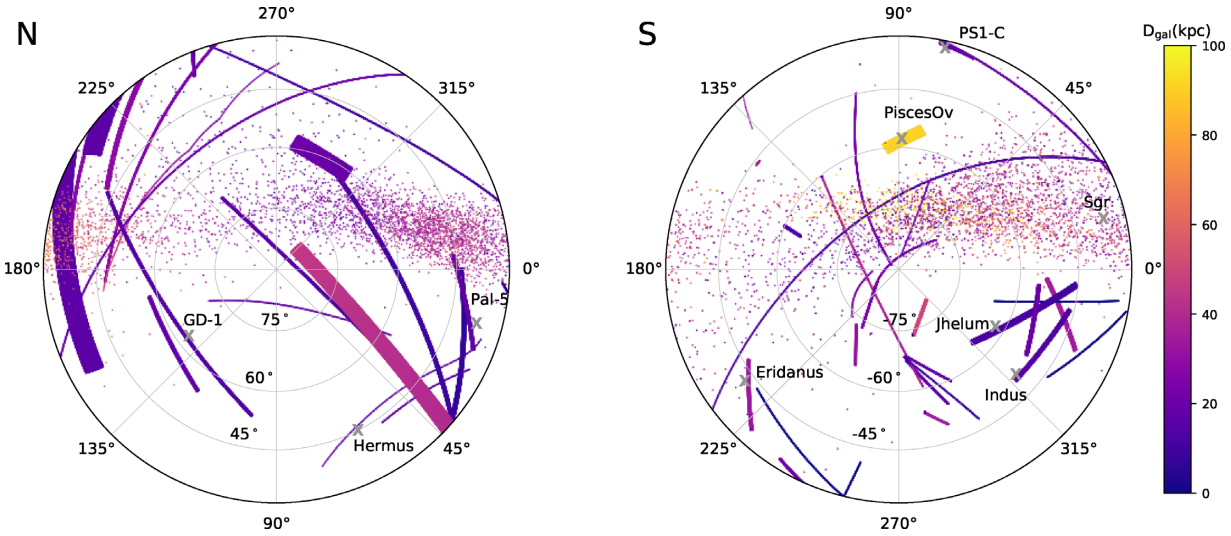

Figure 1. Schematic stellar Stream map of the Milky Way sky prior to Gaia DR2. Here we show the Milky Way stellar stream map (minus some stellar clouds) from the GALSTREAMS package (Mateu et al. 2018), transformed into polar ZEA projections. The colour represents the Galacto-centric distances to these structures. The left- and right-hand panels show, respectively, the projection from the North and South Galactic poles. The names of a few streams are labelled to help the reader's orientation in this coordinate system. Galactic longitude increases clockwise in the north panel and counter-clockwise in the south panel, while Galactic latitude changes radially as shown.

trast) Phlegethon stream in Gaia DR2 with a surface brightness of $\Sigma_G \sim 34.6\,\mathrm{mag\,arcsec^{-2}}$.

The purpose of this contribution is to present an updated stellar stream map of the halo of the Milky Way (at $D_\odot > 5$ kpc) obtained via the application of our STREAMFINDER algorithm onto the recently published Gaia Data Release 2 (DR2, Evans et al. 2018; Gaia Collaboration et al. 2018; Helmi et al. 2018; Lindegren, L. et al. 2018; Luri et al. 2018). In this first analysis, we restrict ourselves to analysing the outer halo at distances beyond 5 kpc as our algorithm takes longer to compute in inner regions, where the density of both the field stars and the possible candidates is large (as is the case when considering closer structures or indeed in the vicinity of the Galactic Plane).

The paper is organized as follows: Section 2 details the selections made on the Gaia data; Section 3 explains how we built a model of the contaminating populations of the Milky Way; the analysis using our STREAMFINDER algorithm is detailed in Section 4; the results are presented in Section 5; finally we discuss these findings and draw our conclusions in Section 6.

2 DATA AND STREAM SEARCH ANALYSIS

We use the Gaia DR2 catalogue for all of our present analysis. This data set provides positions, parallaxes, and proper motions (a 5D astrometric solution) for over 1.3 billion stars down to $G \sim 20.7$ in our Galaxy, along with the Gaia broad-band photometry in the G, $G_{\rm BP}$, and $G_{\rm RP}$ pass-bands. The information that is useful for our purpose are the stellar positions (α, δ), parallaxes (π), proper motions (μ_α, μ_δ), magnitudes (G, $G_{\rm BP}$, and $G_{\rm RP}$), and the associated observational uncertainties.

We correct all Gaia sources from extinction using the Schlegel, Finkbeiner, and Davis (1998) maps, assuming $A_{\rm G}/A_{\rm V} = 0.85926$, $A_{\rm BP}/A_{\rm V} = 1.06794$, and $A_{\rm RP}/A_{\rm V} = 0.65199$.[1] Doing so, we naturally assume that the extinction is entirely in the foreground of the studied stars, which is likely a good assumption for the haloes stars we analyse here. Henceforth, all magnitudes will refer to the extinction-corrected values.

The Gaia DR2 is based on only 22 months of observations, and not all areas of sky have been observed to uniform depth. Gaia scans the sky while spinning, and this naturally imprints great circles into the depth map. In Fig. 2 we show the result of applying an unsharp mask to all data at Galactic latitudes $|b| > 10^\circ$ and with $G < 20$. A large number of stripy residuals can be seen, which could in principle masquerade as streams. Any structures following this pattern are almost certainly artefacts.

After extensive tests of the STREAMFINDER using the Gaia Universe Model Snapshot (GUMS, Robin et al. 2012), we decided to limit the sample for the present contribution to $|b| > 30^\circ$ and $G < 19.5$. The chosen magnitude limit mitigates against the effect of completeness' variations due to inhomogeneous extinction, while also reducing the number of sources that need to be examined. Likewise, the Galactic latitude constraint also greatly diminishes the size of the sample. We retained only those sources that had a full five parameter astrometric solution, along with valid magnitudes in all three photometric bands.

We further omitted all Gaia DR2 catalogue stars within two tidal radii of the Galactic globular clusters listed in the compilation by Harris (2010), as well as all the stars within seven half-light radii around Galactic dwarf satellite galaxies (as compiled by McConnachie 2012). This was implemented so as to avoid creating spurious stream detections that might be caused by the presence of a compact overdensity of stars in a given region of phase space rather than an actual extended stream of stars.

As described in Paper I, it is convenient to reject disc contaminants based on parallax information since we are interested in finding halo structures. The number of these potential nearby contaminants was reduced by removing those sources whose parallax is greater than $1/3000$ arcsec at more than the 3σ level (i.e. objects that are likely to be closer than 3 kpc).

We feed this filtered data to the STREAMFINDER.

[1]These extinction ratios are listed on the Padova model site http://stev.oapd.inaf.it/cgi-bin/cmd_2.8.

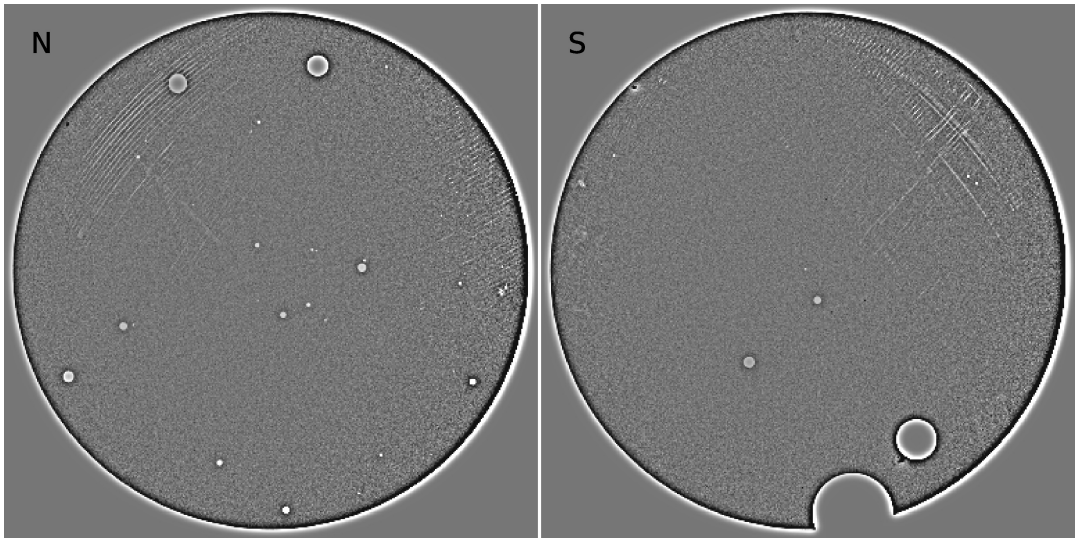

Figure 2. Unsharp-mask map of the $|b| > 10^{\circ}$ sky, derived using Gaia sources brighter than $G_0 = 20$. This simple filtering procedure highlights the stripy artefacts that arise due to the inhomogeneous scanning of the sky in the DR2 catalogue. The same ZEA projections are used here as in Fig. 1. To create this map, we binned the catalogue into pixels of size $5\farcm3 \times 5\farcm3$, and subtracted from this the same map but smoothed with a 2D Gaussian of standard deviation 53 arcmin. The holes seen in the image correspond to the excised regions around known clusters and satellite galaxies that were omitted in our analysis.

3 CONTAMINATION MODEL

Before running the STREAMFINDER, we first calculate an empirical smooth model of the Milky Way 'contamination' (i.e. a model of the smoothly varying population of stars that lie both in the foreground and the background of the stream-like structures of interest). This contamination model is used as a global probability density function estimate to calculate the likelihood function for identifying sub-structures. The procedure will be more fully explained in a future contribution (Ibata et al. 2018, in preparation), but briefly, we construct a library of number-density maps of the Galaxy as a function of $G_{\rm BP} - G_{\rm RP}$ colour, and G magnitude in polar zenithal equal-area (ZEA) projection with a pixel scale of $1\fdg4 \times 1\fdg4$, which are smoothed on a spatial scale of 2°. Furthermore, overspatial regions of $5\fdg6 \times 5\fdg6$ (also in polar ZEA projection), we fit the 4D distribution of $G_{\rm BP} - G_{\rm RP}$ colour, G magnitude, and proper motion μ_α, μ_δ, with a Gaussian mixture model (GMM), with 100 Gaussian components, using the ARMADILLO C++ library (Sanderson & Curtin 2017). Together, the density maps and the GMM fitted maps allow one to estimate the smoothed probability of finding a star in the Galaxy in the 6D parameter space of α, δ, $G_{\rm BP} - G_{\rm RP}$, G, and μ_α, μ_δ.

4 STREAMFINDER ANALYSIS

The STREAMFINDER algorithm is built to detect dynamically cold and narrow tidal stellar streams that are possible remnants of globular clusters or very low mass galaxies. At the position of every star in the data set, the algorithm finds the most likely stream model given the observed phase-space information, and quantifies the likelihood of that stream model given the pre-calculated contamination model. To build the stream model, the algorithm launches orbits from the sky position of the star in question, sampling over the proper motion uncertainties, and over the full range of radial velocity. All possible distances to the star are examined that are consistent with the observed photometry and the chosen stellar populations template. A by-product of the algorithm is the orbital solution of every star along which stream lies (see Paper I for detailed discussion on the workings of the algorithm).

We used the STREAMFINDER to analyse the Gaia DR2 data in a similar way to that described in Paper I. The orbits are integrated within the Galactic potential model 1 of Dehnen and Binney (1998), and these orbits are then projected into the heliocentric frame of observables for comparison with the data. For this coordinate transformation, we assume a Galactocentric distance of the Sun of 8.20 kpc (Karim & Mamajek 2017), a circular velocity $V_{\rm circ} = 240\,{\rm km\,s^{-1}}$, and in addition we adopt the Sun's peculiar velocity to be $\boldsymbol{V}_{\odot} = (u_{\odot}, v_{\odot}, w_{\odot}) = (9.0, 15.2, 7.0)\,{\rm km\,s^{-1}}$ (Schönrich, Binney & Dehnen 2010; Reid et al. 2014). As explained in Paper I, STREAMFINDER uses pre-selected isochrone models in order to sample orbits in distance space. The selected isochrone model(s) essentially correspond to the proposed single stellar population (SSP) model of the stream. Here, we chose to work with Padova SSP models (Marigo et al. 2008) in the Gaia photometric system, with age 10 Gyr and with 7 metallicity values between [Fe/H] $= -2.2$ and [Fe/H] $= -1.0$ (spaced at 0.2 dex intervals). These isochrone models cover plausible values for Milky Way halo globular clusters (from which stellar streams are ultimately derived).[2] The candidate model streams were selected to have a Gaussian width of 100 pc, and to be 10° long on the sky. Other parameter ranges used to integrate orbits in the Galaxy were identical to those detailed in Paper I.

In Paper 1, our analysis was restricted to a small and relatively high-latitude patch of sky ($\sim$100 deg^2) in which the background stellar distribution (the halo) could be approximated as a uniform distribution. In the present case, where we are analysing vast regions of sky that have a non-uniform stellar distribution, it is important to consider the background model of the Galaxy. Therefore, in contrast to Paper I, the likelihood function that we use here takes the Galaxy into consideration via the smooth contamination model discussed

[2]In subsequent papers, we plan to run the algorithm over a fine grid in metallicity and age.

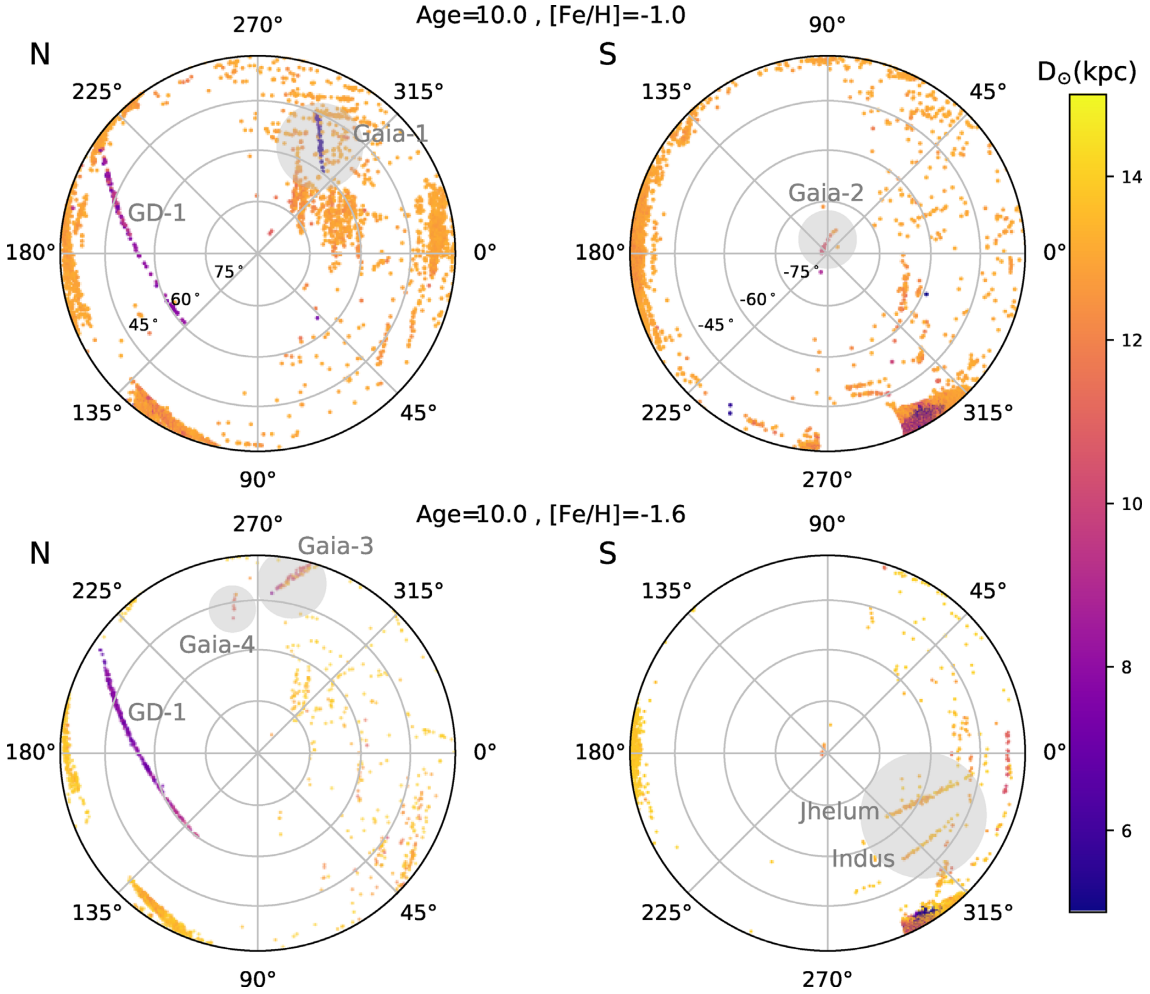

Figure 3. Potential stream stars identified by STREAMFINDER in the inner halo, from 5 to 15 kpc, in the same projection as Fig. 1. The colour represents the distance solutions that are obtained as a by-product for these stars from the STREAMFNIDER analysis. The top panels show a metal-rich selection, while the lower panels show the results for intermediate metallicity. The most striking structure detected in this distance range is the GD-1 stream (Grillmair & Dionatos 2006), seen clearly towards the lower end of the distance range (coloured purple) in the Northern hemisphere (left-hand panels). Several other streams are visible, including the Jhelum and Indus streams discovered in the DES (Shipp et al. 2018). All stream points displayed here have detection significance $>5\sigma$. New high-confidence stream detections are marked on the map, while the others will require confirmation with radial velocity measurements.

above. Our log-likelihood function is simply:

$$\ln\mathcal{L} = \sum_{\text{data}} \ln\left(\eta\mathcal{P}_{\text{signal}}(\theta) + (1-\eta)\,\mathcal{P}_{\text{contamination}}\right), \quad (1)$$

where θ are the stream fitting parameters, $\mathcal{P}_{\text{contamination}}$ is the probability density function of the smooth contamination model that we obtain as explained in Section 3, and η is the fraction of the stream model compared to the contamination. The adopted stream probability density function, $\mathcal{P}_{\text{signal}}$, is extremely simple: We take the trial orbit under consideration and make it fuzzy by convolving it with a Gaussian in each observed dimension. The Gaussian dispersions are: σ_{sky} representing the thickness of the stream, σ_{μ_α}, σ_{μ_δ} representing the dispersions in proper motion, and σ_{DM} representing the dispersion in distance modulus (and hence in photometry). All these dispersions are the convolution of the intrinsic Gaussian dispersion of the stream model together with the observational uncertainty on each star in the Gaia DR2 catalogue.

5 RESULTS

In Fig. 3 we show, for two representative metallicity values, the spatial distribution of the stars in the processed sample that has a high likelihood of belonging to a stream structure. These data are selected as having $\ln\mathcal{L}_{\text{max}}/\ln\mathcal{L}_{\eta=0} > 15$, where $\mathcal{L}_{\eta=0}$ is the model likelihood when no stream is present, and $\mathcal{L}_{\text{max}}$ is the maximum likelihood stream solution found by the algorithm. Thus, our criterion corresponds to $>5\sigma$ when the noise distributions are Gaussian. We would like to point out that the $\ln\mathcal{L}_{\text{max}}/\ln\mathcal{L}_{\eta=0}$ likelihood ratio is calculated for every star in the (filtered) catalogue, yet in the maps presented here we only show those stars where this value exceeds 15. Many other neighbouring stars may partake in a given stream structure, contributing to the high $\ln\mathcal{L}_{\text{max}}/\ln\mathcal{L}_{\eta=0}$ valued points marked in the figure, yet they may not themselves pass the criterion and so are not shown. A given stream-like structure seen in the figure is thus composed of many $>5\sigma$ points. However, the points are not statistically independent, as by construction

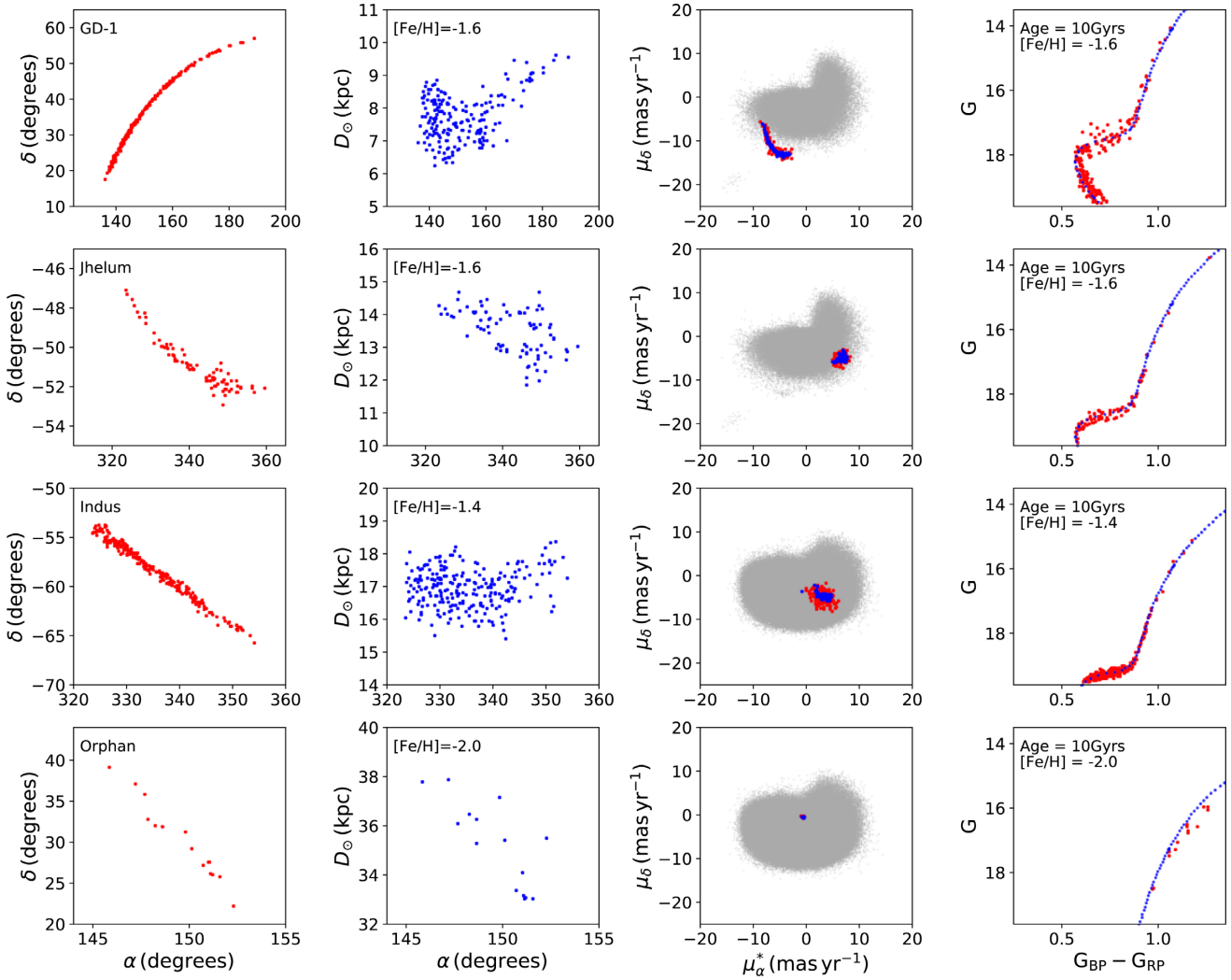

Figure 4. Properties of a sample of previously discovered streams, as recovered by the STREAMFINDER. The first, second, third, and fourth rows show the properties of the GD-1, Jhelum, Indus, and Orphan streams, respectively. The columns reproduce, from left to right, the equatorial coordinates of the structures, the distance solutions found by the algorithm (for representative metallicity values), the proper motion distribution (with observations in red, model solutions in blue, and the full DR2 sample in grey), and the colour-magnitude distribution of the stars (with observations in red and template model in blue) selected by STREAMFINDER. The distance solutions found by the algorithm match closely the distance values that have been previously derived for these streams: $D_\odot \sim 8$ kpc for GD-1 (Grillmair & Dionatos 2006), $D_\odot \sim 13.2$ kpc and $\sim$16.6 kpc for Jhelum and Indus, respectively (Shipp et al. 2018), and $D_\odot = [33 - 38]$ kpc for Orphan (Newberg et al. 2010). The CMD template models, shown in blue in the last column, have been plotted at the appropriate distance for the respective streams. The colour-magnitude diagram of the Orphan stream might seem peculiar, but here we only see the red-giant branch due to the trimming of the data sample below $G = 19.5$.

information is correlated over the chosen 10° trial stream length. We further stress that the aim of the STREAMFINDER algorithm is to enable the detection of streams; a complete characterization and statistical analysis of a given detection should be accomplished with other tools, for instance, by careful modelling with N-body simulations.

The left- and right-hand panels of Fig. 3 show, respectively, the projection from the North and South poles. The distance solutions displayed here are the ones obtained by the algorithm and span the inner halo range $D_\odot = [5, 15]$ kpc. The most visible feature in the northern hemisphere is the GD-1 stellar stream (Grillmair & Dionatos 2006; de Boer et al. 2018), which appears as a >60° stream in these spatial density maps of candidate stream members. It is possible that it continues to lower Galactic latitude, where we have not yet run the algorithm. Other notable detections are the Jhelum and Indus streams (Shipp et al. 2018) seen in the Southern hemisphere in the more metal-poor map. As a demonstration of the power of the algorithm, we display the properties of GD-1, Jhelum and Indus, as recovered by the STREAMFINDER, in Fig. 4. Note that the distance solutions to these streams that we obtain from STREAMFINDER match closely the distance values that have been previously derived for these streams (as explained in Fig. 4). The scatter in the distance solutions that is notably seen for individual streams could be a combination of the true intrinsic dispersion of the stream and errors from mismatches with the isochrone template model (from which the distance solutions are derived, see Paper I).

Table 1. Parameters of the stellar streams. The 'Position' column gives the extent of these structures, '$D_\odot$' is the approximate range of the distance solution as obtained by our algorithm, while column 4 lists the range of observed proper motion of the structure in the 2D proper motion space. The parallax π is an uncertainty weighted average of the Gaia measurements; for those objects where the parallax uncertainty is less than 33% of the parallax, we also provide the corresponding distance. The discrepancy between the model distances and mean parallax measurement for the cases of Indus and Gaia-5 may be due to contaminants in the samples affecting the simple weighted average parallax reported here.

Name	Position (extent)	$D_\odot$ (model) (kpc)	$(\mu_\alpha^*, \mu_\delta)$ (mas yr^{-1})	π (mas)	$\frac{1}{\pi}$ (kpc)
GD-1	$135^\circ < \alpha < 190^\circ$ $17^\circ < \delta < 58^\circ$	6.5–10	([−9.0, −3.0], [−14.0, −6.0])	0.107 ± 0.010	9.3
Jhelum	$320^\circ < \alpha < 360^\circ$ $-53^\circ < \delta < -47^\circ$	11.7–15	([5.0, 8.0], [−7.0, −3.0])	0.086 ± 0.013	11.6
Indus	$320^\circ < \alpha < 360^\circ$ $-67^\circ < \delta < -53^\circ$	16–18	([0.50, 6.0], [−8.0, −2.0])	0.167 ± 0.013	6.0
Orphan	$145^\circ < \alpha < 153^\circ$ $20^\circ < \delta < 40^\circ$	33–38	([−1.0, −0.5], [−0.7, −0.1])	−0.006 ± 0.022	
Gaia-1	$184^\circ < \alpha < 197^\circ$ $-18^\circ < \delta < -2^\circ$	5–6	([−16.0, −11.0], [−22.0, −17.0])	0.216 ± 0.038	4.6
Gaia-2	$6^\circ < \alpha < 15^\circ$ $-27^\circ < \delta < -22^\circ$	10–13	([2.7, 5.4], [−6.0, −4.0])	0.117 ± 0.062	
Gaia-3	$171^\circ < \alpha < 179^\circ$ $-32^\circ < \delta < -15^\circ$	9–14	([−2.0, 1.0], [−9.3, −5.5])	0.101 ± 0.013	9.9
Gaia-4	$163^\circ < \alpha < 167^\circ$ $-11^\circ < \delta < -3^\circ$	10.7–11.5	([−1.1, 0.5], [−1.1, 0.6])	0.006 ± 0.105	
Gaia-5	$137^\circ < \alpha < 154^\circ$ $23^\circ < \delta < 42^\circ$	18.5–20.5	([−4.0, 1.5], [−5.7, −1.5])	0.156 ± 0.031	6.4

We summarize some of the properties of these structures in Table 1, providing, for the first time, the proper motion values for the Jhelum and Indus streams.

The recovery of known stellar streams provides validation of our algorithm. Many other stream-like features can also be seen in this map, but these structures require detailed kinematic analysis for their confirmation (which is beyond of the scope of this paper). In the present contribution we will discuss the most obvious stream structures that not only have coherent phase-space properties (consistent with the template model and the data uncertainties) but that also stand out significantly from the background. These new streams, that are named Gaia-1,2,3,4, are shaded in grey in Fig. 3 and their phase-space properties are presented in Fig. 9.

Fig. 5 shows the results at intermediate distances in the halo in the range $D_\odot = [15, 30]$ kpc (again selecting $\ln\mathcal{L}_{\max}/\ln\mathcal{L}_{\eta=0} > 15$). Unlike Fig. 3 that exhibits clearly distinguishable stream-like strings of stars, these maps produced at intermediate distances are rather fuzzy and only seldom show thin stream-like features. Some of these stream features become apparent in the regions $|b| > 45^\circ$, where the density of contaminating stars is low. The most obvious stream structure is Gaia-5, which is shaded in the grey circle in Fig. 5 and its phase-space properties are presented in Fig. 9.

The outer halo distribution, beyond 25 kpc is displayed in Fig. 6 (again selecting $\ln\mathcal{L}_{\max}/\ln\mathcal{L}_{\eta=0} > 15$). The algorithm highlights a veritable deluge of stream-like structures, which are seen over a range of distances and metallicities. Comparison to Fig. 1 shows that we detect the Sagittarius stream (Ibata et al. 2001; Majewski et al. 2003) over a large swathe of the outer halo. This is somewhat surprising, since we set the stream model width to 100 pc, which is appropriate for a globular cluster, but is actually a very poor template for this wide stream. We suspect that the spatial inhomogeneities in Gaia due its scanning law may partially explain the striated aspect of the Sagittarius stream in our maps (see e.g. Fig. 6). The algorithm also detected a short arc of length $\sim 10^\circ$ of the $\sim 60^\circ$ long Orphan stream (Grillmair 2006) in our outer halo spatial maps (again, the chosen stream width of the model was not an appropriate template for this structure, which may explain why the full length was not recovered). For the position of the arc on the sky shown in Fig. 4, we find the distance solutions for the Orphan stream members to be compatible with the study by Newberg et al. (2010). Also, we find that its member stars have a tight proper motion distribution (Table 1 provides proper motion values for the Orphan stream). This map also requires follow-up with radial-velocity measurements in order to test the phase-space consistency of the other possible stream-like structures that are distributed on these maps (for example, see the bottom panels of Fig. 6).

Careful visual inspection of these maps indicated that the stream-like structures recovered by the algorithm are not associated with the extinction correction. In Figs 7 and 8, we present our summary plots made by combining the distance and metallicity samples for the north and south hemispheres, respectively. The top panels of these diagrams show the estimate of the distances of these structures (provided by the algorithm), while the bottom panels show an estimate of the magnitude of the tangential velocity calculated using the measured Gaia proper motions combined with the distance estimates. Many structures are beautifully resolved in this multiparameter space.

Our aim in this contribution is not to present a thorough or complete census of halo streams (since it would require considerably more processing time to examine the necessary parameter space), but rather to present a preview of the large-scale stream structure of our Galaxy. Nevertheless, we have selected by hand a small number of structures that appear clearly in our maps, with kinematic properties that distinguish them from the contaminating Galactic population, and that are clearly not artefacts produced by Gaia's scanning law. A large number of other stream candidates

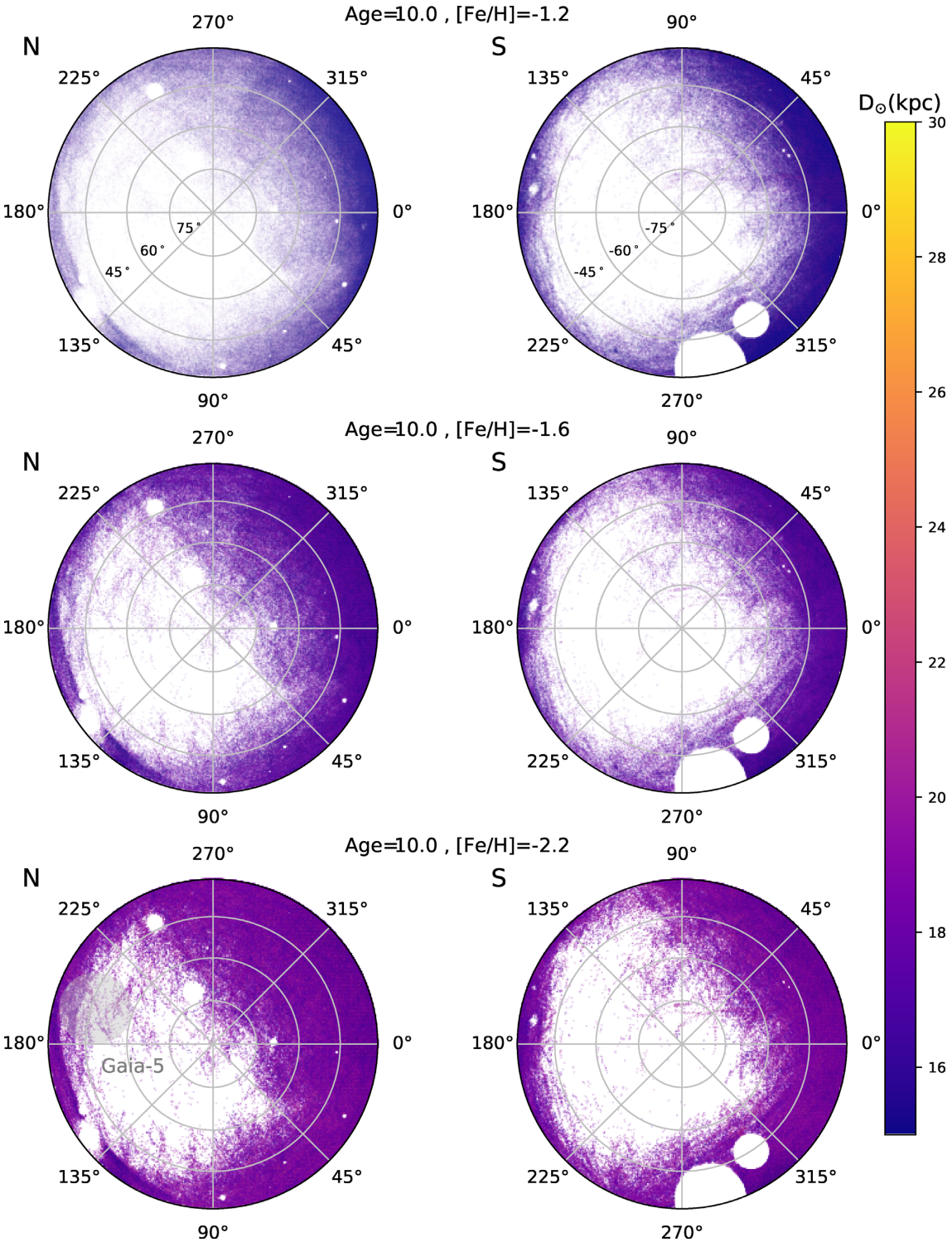

Figure 5. Spatial distribution of stream candidates at intermediate distances. Here we show the stellar stream density map as obtained from the STREAMFINDER based on three representative isochrone models. Each row corresponds to a particular isochrone model of age (in Gyr) and metallicity, as labelled. The left-hand panels represent the North side of the ZEA projection system and the right-hand panels represent the South. The colour scale is proportional to the heliocentric distances to the stellar members of the detected structures obtained as a by-product from the STREAMFINDER analysis. All streams displayed here have detection significance $>5\sigma$. New high-confidence stream detections are marked on the map.

have a clearly-defined stream-like morphology, but possess proper motions distributions that are similar to that of the halo, and we deem that they require further follow-up to be confident of their nature.

The locations of the five structures we selected are marked in Figs 3 and 5, and their properties are shown in Fig. 9 and are also summarized in Table 1. All these structures that we find have significance $>5\sigma$.

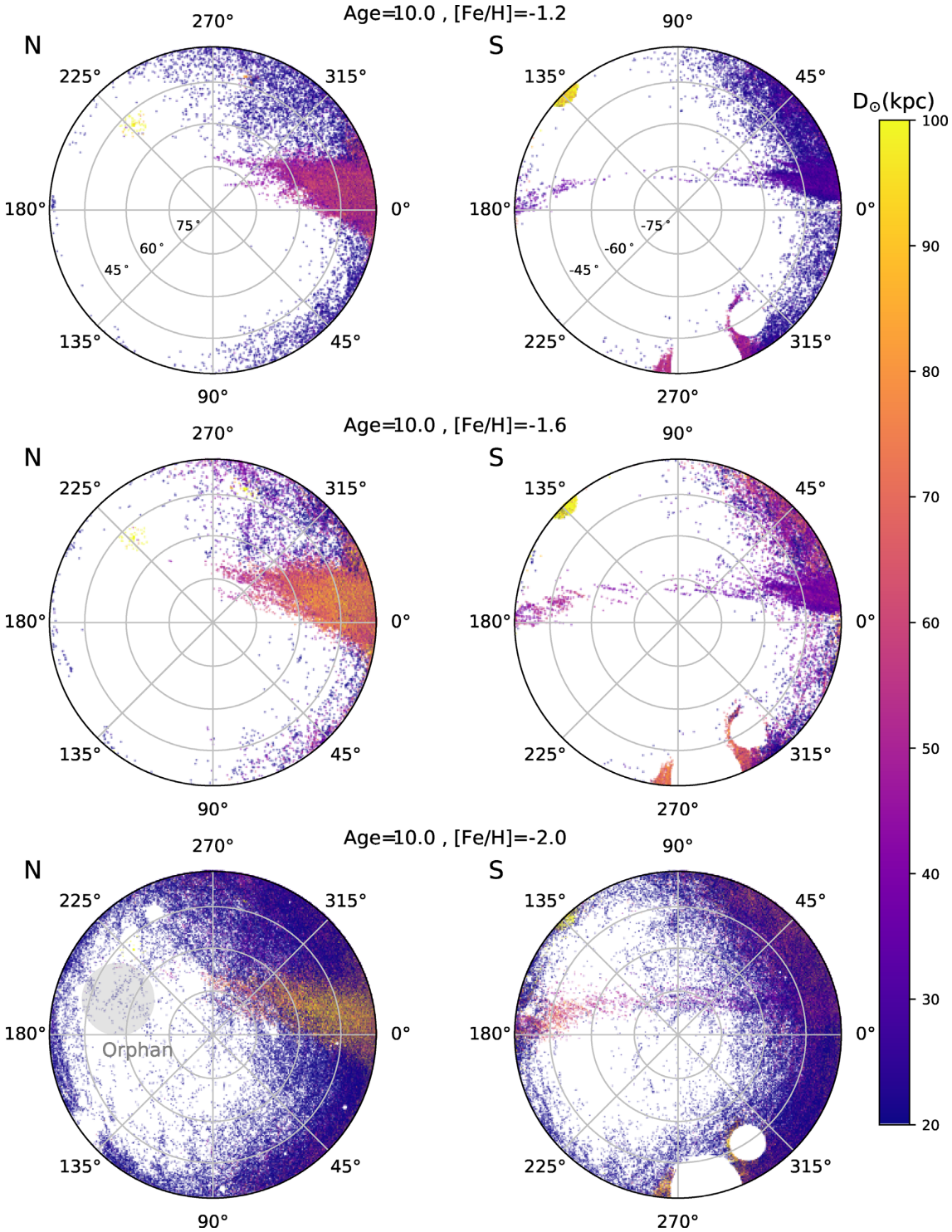

Figure 6. As Fig. 5, but for the outer halo beyond 25 kpc. The dominant structure seen out to large heliocentric distances in both hemispheres is the Sagittarius stream, which is detected despite the narrowness of the stream template model that we set in our algorithm. The interesting bifurcation of this structure is seen in the top-left panel. In addition, the lower left panel shows an overdensity of stars in the region where the Orphan stream lies (Grillmair 2006). Many other stream-like features are also detected, but most are confined to the nearer limit of the distance range shown.

5.1 Gaia-1

Gaia-1 has an angular extent of $\sim$15° and projected width of $\sim$0.5°. The orbital solutions provided by the algorithm imply that it is situated at a distance of $D_\odot \sim 5.5$ kpc, which is in reasonable agreement with the Gaia parallax measurement of 0.216 ± 0.038 mas (i.e. 4.6 kpc). This means that Gaia-1 has a physical width of $\sim$40 pc. The narrowness of the stream suggests that the progenitor likely is or was a globular cluster. Moreover, Gaia-1 has a strikingly high proper motion value of $\sim$23.5 mas yr^{-1}, implying that it has a transverse motion $\gtrsim$500 km s^{-1}. It will be worthwhile to measure the

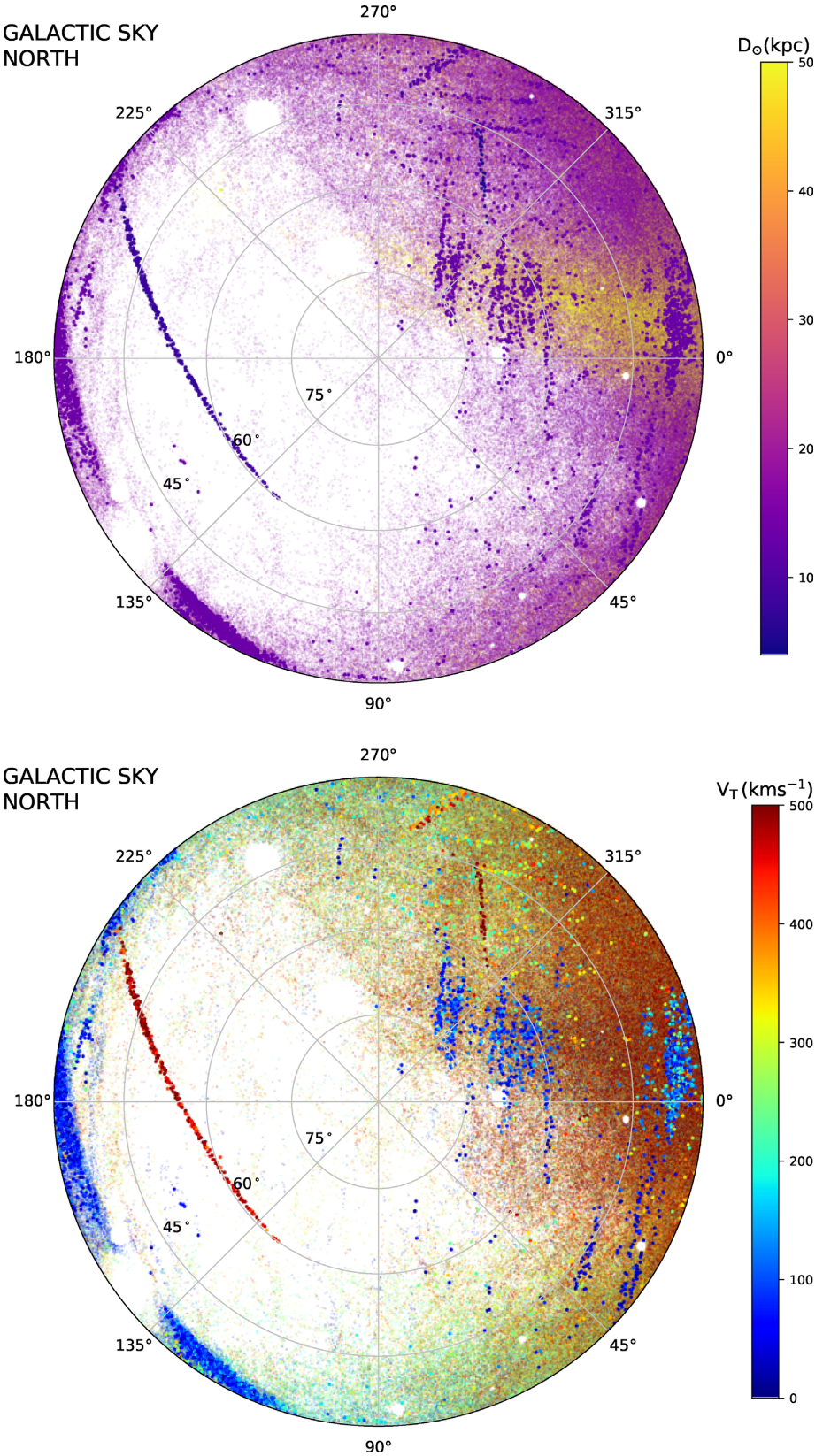

Figure 7. Summary diagrams of the distance ($D_{\odot} > 5$ kpc) and tangential velocity V_T of stream-like structures in the northern Galactic sky. The tangential velocities are calculated based on the observed proper motion of the stars in DR2 and the corresponding distance estimates that we obtain from the algorithm. Most of the structures that we report here are visible in these diagrams, as are many others that we intend to investigate further in future contributions.

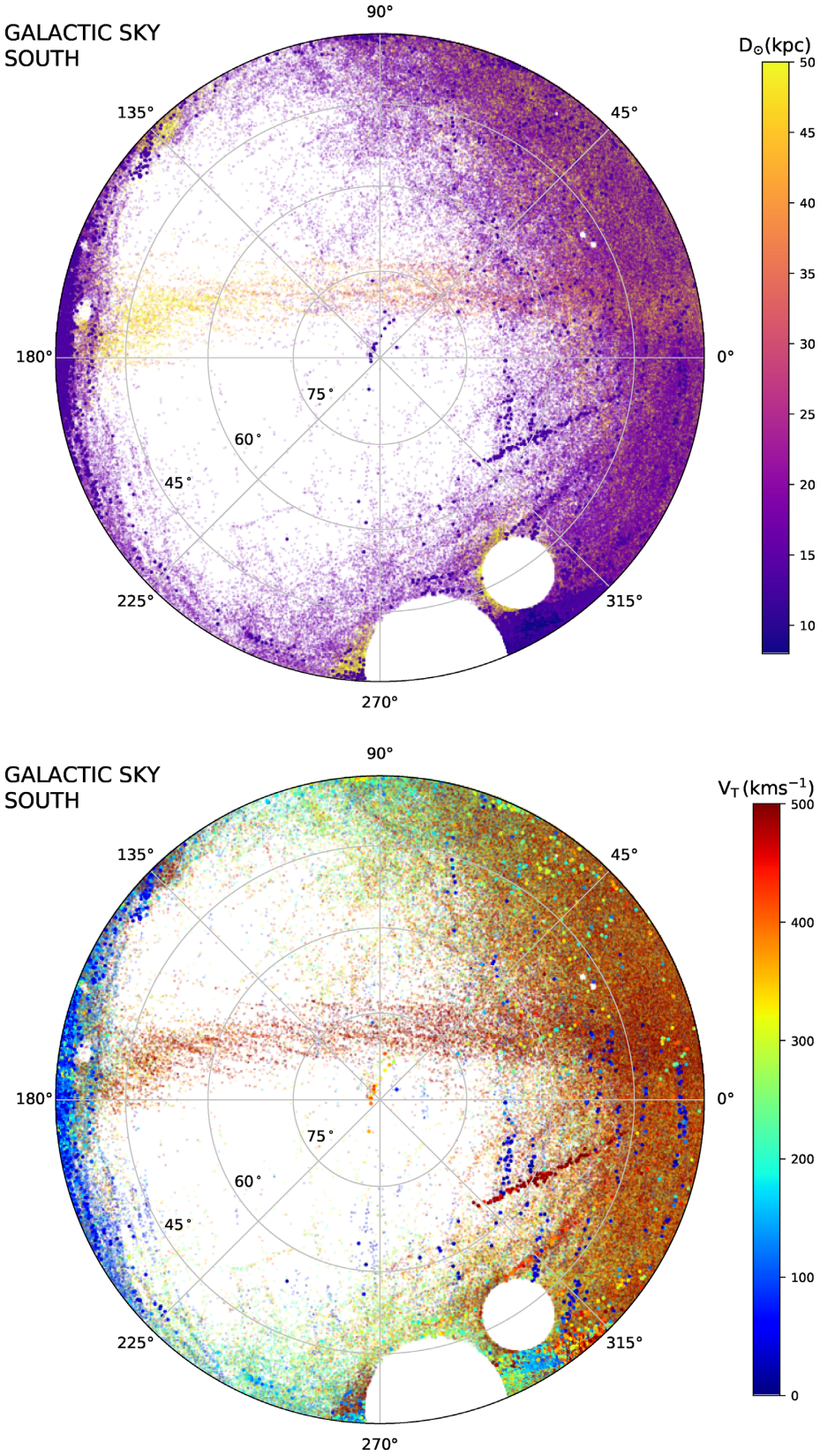

Figure 8. As Fig. 7, but for the southern Galactic sky.

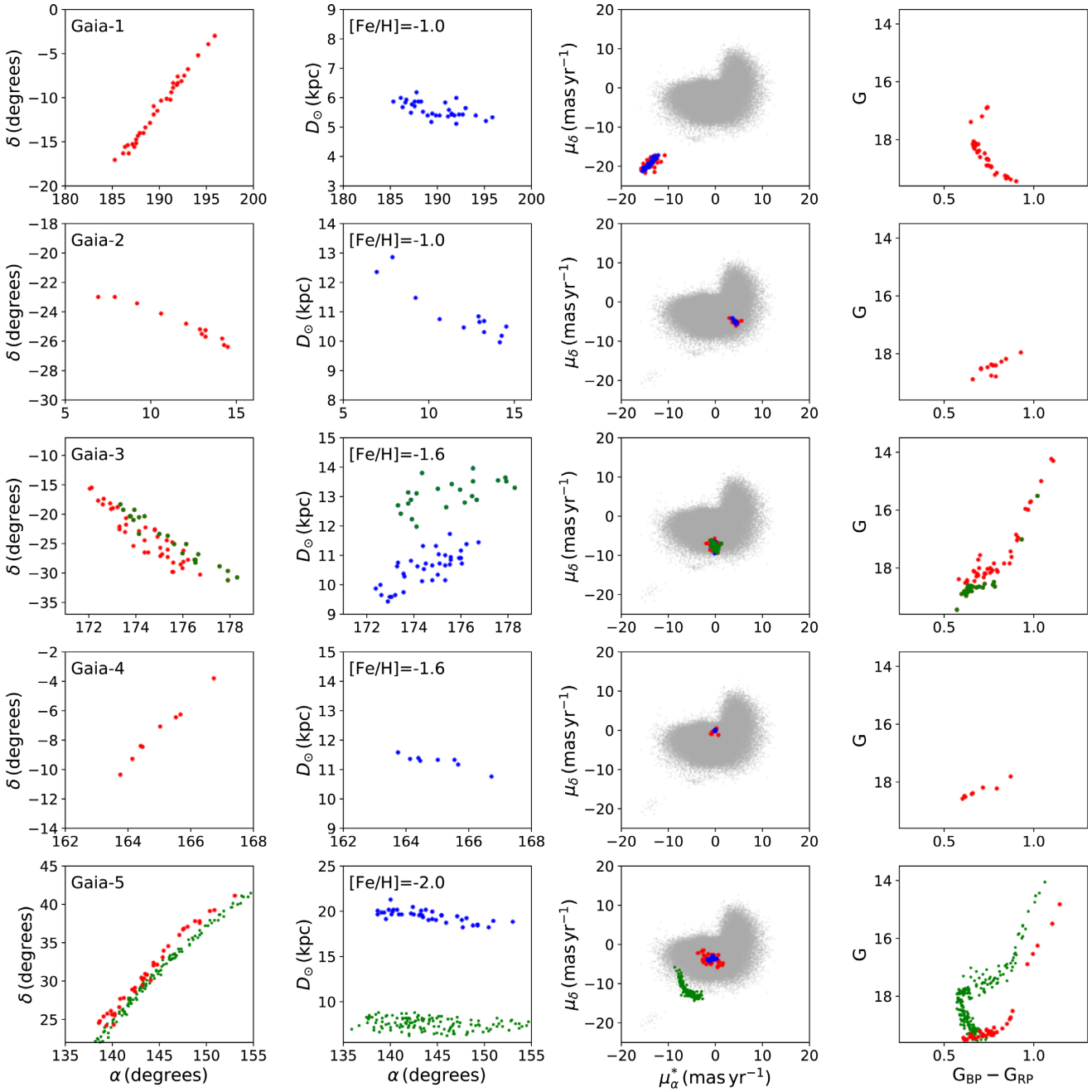

Figure 9. As Fig. 4 but for the selected set of newly-discovered streams. Oddly, for Gaia-3, we found two distinct possible sets of solutions based on distance estimates that we obtained from our algorithm, as highlighted in the respective panel. The more distant stars are coloured in green, while the relatively nearby ones are shown in red. This clear distinction of these two different sets of solutions in position, distance, and colour-magnitude distribution space, while not so much in proper motion space, suggests that what we detect here as Gaia-3 might in fact be a superposition of two streams, or a more complicated structure aligned along the line of sight. The bottom row shows the properties of Gaia-5, which is found to lie parallel, but slightly offset, to GD-1 (shown on this bottom row in green). Nevertheless, it is very distinct from GD-1 both in its proper motion distribution and in its colour-magnitude distribution.

radial velocity of this system, as it may provide an interesting constraint on the Galactic potential simply from the requirement that the system is bound to the Milky Way.

5.2 Gaia-2

Gaia-2 turns out to be a considerably thin structure in our spatial maps. Extending over $\sim 10^\circ$ in length, we find that it possesses a distance gradient ranging from $D_\odot = [10\text{–}13]$ kpc. Given its narrowness and the location in the halo, we also suspect it to be a remnant of a globular cluster. We find Gaia-2 to be a highly coherent structure in proper motion space with an average proper motion magnitude of ~ 6.5 mas yr^{-1} and proper motion dispersion of ~ 0.75 mas yr^{-1}.

5.3 Gaia-3

Gaia-3 can be easily identified as an isolated stream structure in Fig. 3. In Fig. 9 (third row), Gaia-3 clearly shows two distinct possible sets of distance solutions. The separation of these two

different sets of solutions in position, distance and colour-magnitude distribution (CMD) space, while not so much in proper motion space, suggests that what we detect here as Gaia-3 might in fact be a superposition of two streams, or a more complicated structure aligned along the line of sight. We shall describe this structure collectively here.

Gaia-3 is found to be extended over $\sim 16^\circ$ in sky with a distance range of $D_\odot = [9–14\,\mathrm{kpc}]$ with an average proper motion magnitude of $\sim 7.4\,\mathrm{mas\,yr^{-1}}$. Given its peculiarity, as suggested above and shown in Fig. 9, it is hard to comment on its physical width or the progenitor. The distance estimate of this structure too was found to be in good agreement with the Gaia parallax measurement of 0.101 ± 0.013 mas (i.e. 9.8 kpc).

5.4 Gaia-4

Gaia-4 appears to be a fine linear structure, found at a distance of $\sim D_\odot = 11$ kpc. Given its narrowness and distance, we suspect the progenitor to be a globular cluster. Although we find Gaia-4 sitting within the range of halo field stars in proper motion space with an average value of $\sim 0.36\,\mathrm{mas\,yr^{-1}}$ (and proper motion dispersion of $\sim 0.70\,\mathrm{mas\,yr^{-1}}$), the fact that it emerges as a highly coherent structure in our maps makes it a confident structure. Here, we detect it as a very cold structure in proper motion space.

5.5 Gaia-5

We include Gaia-5 here as another interesting detection (bottom row panels in Fig. 9), as it is parallel to the GD-1 stream, and could easily have been confused with GD-1 without Gaia's excellent proper motion measurements. The properties of this object are shown in red for positions, observed proper motions, and photometry, and in blue for distance and proper motion orbital solutions. We also include the properties of GD-1 (in green) for comparison. The proper motions, along with the distance solutions, of Gaia-5 stars are distributed over a compact region that is very far from the region inhabited by GD-1; also the two CMDs are very different and well separated. Hence, unlike the possible bimodal stream distribution that we recognize in Gaia-3, we identify Gaia-5 as a stream unrelated to GD-1. The (error-weighted mean) parallax value we calculate for this structure would imply that it is substantially closer to the Sun than GD-1, which is both inconsistent with the model solutions of ~ 20 kpc, and is very difficult to reconcile with the CMD. However, our simple combination of the parallax measurements is highly susceptible to contaminants, which may explain the inconsistency.

We plan to examine these structures (and the many other stream candidates visible in Figs 7 and 8) in detail in later contributions. Careful analysis based on their astrometry and photometry, along with the mapping of these structures in deeper astrophysical catalogues (e.g. SDSS, PS1, and DES), would render a fuller insight into their origin, orbits, and phase-space distribution. Some of the previously known streams and new detections appear to present spatial kinks, which is probably the effect of low-number statistics.

6 DISCUSSIONS AND CONCLUSIONS

In this contribution, we present a new stellar stream map of the Milky Way halo, obtained by the application of our STREAMFINDER algorithm (described in Paper I) on the recently published ESA/Gaia DR2 catalogue. This is the first time an all-sky structural and kinematic map of the stellar streams of the Milky Way halo has been constructed. Our algorithm detects numerous previously known streams, which were discovered in much deeper photometric data sets (e.g. SDSS, PS1, and DES), confirming that our method, which includes proper motion information, works as designed. Indeed, the fidelity of the GD-1 detection is striking, and reveals that the excellent Gaia proper motions provide very powerful discrimination.

In addition, we find a large number of streams and stream candidates throughout the distance range probed. In this first exploration, we selected five good streams (named here as Gaia-1,2,3,4,5), to showcase the results, but many other candidates will require careful follow-up. In particular, the fact that Gaia scans the sky along great circles, but with an inhomogeneous number of visits, causes density inhomogeneities that appear like great circle streaks on the sky. This could cause some spurious stream detections (although the kinematics test in the STREAMFINDER algorithm should allow us to reject most such fake streams). Nevertheless, these spatial inhomogeneities in the Gaia DR2 necessarily make the survey noise properties very complex, invalidating the assumptions behind our $\ln\mathcal{L}_{\max}/\ln\mathcal{L}_{\eta=0} > 15$ selection criterion. This means, unfortunately, that the effective stream detection threshold is not uniform in our sky maps, and the significance of the detections is lower in regions where the Gaia inhomogeneities are more pronounced.

A further caveat relates to the model distances we report. These distances are calculated by the algorithm based on an assumption of the metallicity of the stream stars. We expect that we do, in fact, have some ability to estimate the metallicity of the candidate streams with our procedure, since using the correct metallicity model should enhance the contrast of the streams. This is borne out, for instance, for the case of GD-1, where we recover the largest number of stream stars when using the model corresponding to the actual metallicity of the system. Nevertheless, this is a poor substitute for actual metallicity measurements. Ongoing sky surveys, such as the Canada–France Imaging Survey (CFIS; Ibata et al. 2017a,b), or future large photometric surveys such as LSST (LSST Dark Energy Science Collaboration 2012), can help overcome this issue by providing good photometric metallicities that will break the distance degeneracy (and improve stream detection). The third Gaia data release (DR3), currently planned for 2020, will provide low-resolution prism spectra, also allowing metallicity measurements for the brighter stars.

As we showed in Paper I, our algorithm naturally delivers the possible set of orbital solutions of the detected stream structures. This means that the algorithm predicts both the radial velocities and the distances of the stream stars. In Fig. 10 we use the orbital solutions to the GD-1 stream to demonstrate that this works very well: the predicted STREAMFINDER radial velocities match the stream velocities measured by Koposov et al. (2010). Furthermore, our parallax measurement of 0.107 ± 0.010 mas for GD-1, based on the sample we obtain with the STREAMFINDER, also matches well the distance range of the orbital solutions shown in Fig. 4 (these are not independent measurements, however, the algorithm 'sees' the potential stream stars diluted in a gigantic Galactic contaminating population). This success gives us confidence that we will be able to use the predicted STREAMFINDER radial velocities to probe the orbital properties of the stellar stream population as a whole.

Several more streams have been reported within 40 kpc than the five that we recover here (see Fig. 1). The reason for this is likely to be due, in part, to the specific parameter choices we adopted in the algorithm (for instance we chose a model width of 100 pc throughout, and we examined only a narrow range of stellar population template models). In subsequent contributions, we intend to relax these constraints allowing for a more complete census to be established. Additionally, we intend to examine different models of the

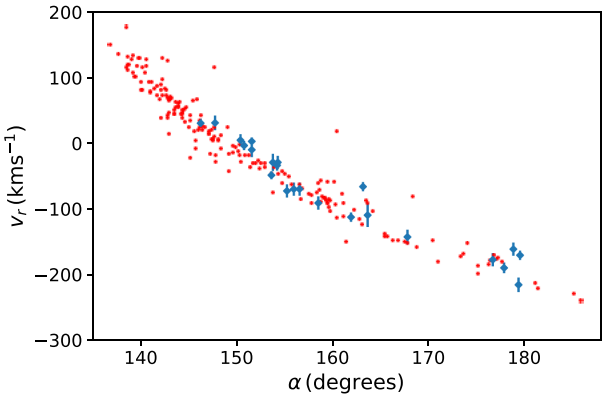

Figure 10. Predicting the missing phase-space information of streams stars with STREAMFINDER. The red dots represent the radial velocity solutions of the GD-1 stars that are derived as a by-product of the application of the algorithm, whereas the blue markers are the observed radial velocities of GD-1 stars as tabulated by Koposov et al. (2010). The STREAMFINDER sampled orbits in radial velocity space at intervals of 10 km s^{-1} (which effectively causes an uncertainty of 10 km s^{-1} on the red dots). The good agreement with the observations illustrates the power of our algorithm in predicting the missing phase-space information of stream stars.

Galactic potential; presumably, our stream detection method should reveal the highest contrast for long stellar streams when using the correct potential. However, another reason that we did not recover all known streams within 40 kpc is simply that Gaia's photometry is not as deep as existing sky surveys; note that for a stellar population of metallicity [Fe/H] $= -1.5$, the distance at which the proper motion uncertainties in Gaia DR2 at the main-sequence turn-off are 50 km s^{-1} (i.e. approximately half the dispersion of the contaminating halo) is 14.0 kpc. Hence it is not very surprising that photometric surveys that are much deeper than Gaia remain competitive for finding low-mass stellar streams at distances $\gtrsim$15 kpc.

Thanks to the amazingly rich phase-space information provided by the Gaia spacecraft and consortium, we are now starting to unravel the very fine details of galaxy formation in action. While the results presented here are but a first step in the comprehensive mapping of the Milky Way's stellar halo and accretion events, they already show the promises borne out by the deep, multidimensional space unveiled in DR2. The harvest of previously unknown thin stellar streams, likely stemming from the tidal disruption of globular clusters, opens up exciting times as these are powerful probes of the distribution of dark matter sub-haloes in our surroundings (Ibata et al. 2002; Johnston et al. 2002; Carlberg et al. 2012; Bovy 2016); they can provide an independent inference of the location of the Sun in phase space (Malhan & Ibata 2017); they can be used as sensitive seismographs to constrain the shape and depth of the Milky Way potential (Ibata et al. 2013; Bonaca & Hogg 2018). The combination of Gaia DR2 and detections provided by `streamfinder` places us in a unique position to disentangle the numerous detections accretion events in the Milky Way halo and open the most exciting Galactic archaeology playground to date.

ACKNOWLEDGEMENTS

We thank the anonymous referee very much for their helpful comments.

This work has made use of data from the European Space Agency (ESA) mission *Gaia* (https://www.cosmos.esa.int/gaia), processed by the *Gaia* Data Processing and Analysis Consortium (DPAC, https://www.cosmos.esa.int/web/gaia/dpac/consortium). Funding for the DPAC has been provided by national institutions, in particular the institutions participating in the *Gaia* Multilateral Agreement.

The authors would like to thank Michel Ringenbach of the HPC centre of the Université de Strasbourg for his kind support. We also acknowledge support by the Programme National Cosmology et Galaxies (PNCG) of CNRS/INSU with INP and IN2P3, co-funded by CEA and CNES. NFM gratefully acknowledges the Kavli Institute for Theoretical Physics in Santa Barbara and the organizers of the 'Cold Dark Matter 2018' program, during which some of this work was performed. This research was supported in part by the National Science Foundation under Grant No. NSF PHY11-25915

REFERENCES

Balbinot E., Gieles M., 2018, MNRAS, 474, 2479
Belokurov V. et al., 2006, ApJ, 642, L137
Bernard E. J. et al., 2014, MNRAS, 443, L84
Bonaca A., Hogg D. W., 2018, preprint (arXiv:1804.06854)
Bovy J., 2016, Phys. Rev. Lett., 116, 121301
Bovy J., Bahmanyar A., Fritz T. K., Kallivayalil N., 2016, ApJ, 833, 31
Bullock J. S., Boylan-Kolchin M., 2017, ARA&A, 55, 343
Carlberg R. G., Grillmair C. J., Hetherington N., 2012, ApJ, 760, 75
de Boer T. J. L., Belokurov V., Koposov S. E., Ferrarese L., Erkal D., Côté P., Navarro J. F., 2018, MNRAS, 477, 1893
de Bruijne J. H. J., 2012, Ap&SS, 341, 31
Dehnen W., Binney J., 1998, MNRAS, 294, 429
Erkal D., Belokurov V., Bovy J., Sanders J. L., 2016, MNRAS, 463, 102
Evans D. W. et al., 2018, A&A, 616, 21
Eyre A., Binney J., 2009, MNRAS, 400, 548
Gaia Collaboration, 2016, A&A, 595, A2
Gaia Collaboration, 2018, A&A, 616, 22,
Gaia Collaboration, 2018, A&A, 616, 47
Grillmair C. J., 2006, ApJ, 645, L37
Grillmair C. J., Carlin J. L., 2016, in Newberg H. J., Carlin J. L., eds, Astrophysics and Space Science Library Vol. 420, Tidal Streams in the Local Group and Beyond. Springer, Switzerland, p. 87
Grillmair C. J., Dionatos O., 2006, ApJ, 643, L17
Harris W. E., 2010, preprint (arXiv:1012.3224)
Helmi A., White S. D. M., 1999, in Gibson B. K., Axelrod R. S., Putman M. E. eds, ASP Conf. Ser. Vol. 165, The Third Stromlo Symposium: The Galactic Halo. Astron. Soc. Pac., San Francisco, p. 89
Ibata R., Lewis G. F., Irwin M., Totten E., Quinn T., 2001, ApJ, 551, 294
Ibata R. A., Lewis G. F., Irwin M. J., Quinn T., 2002, MNRAS, 332, 915
Ibata R., Lewis G. F., Martin N. F., Bellazzini M., Correnti M., 2013, ApJ, 765, 5
Ibata R. A. et al., 2017a, ApJ, 848, 12
Ibata R. A. et al., 2017b, ApJ, 848, 20
Ibata R. A., Malhan K., Martin N. F., Starkenburg E., 2018, preprint (arXiv:1806.01195)
Johnston K. V., Hernquist L., Bolte M., 1996, ApJ, 465, 278
Johnston K. V., Zhao H., Spergel D. N., Hernquist L., 1999, ApJ, 512, L109
Johnston K. V., Spergel D. N., Haydn C., 2002, ApJ, 570, 656
Karim M. T., Mamajek E. E., 2017, MNRAS, 465, 472
Koposov S. E., Rix H.-W., Hogg D. W., 2010, ApJ, 712, 260
Küpper A. H. W., Balbinot E., Bonaca A., Johnston K. V., Hogg D. W., Kroupa P., Santiago B. X., 2015, ApJ, 803, 26
Law D. R., Majewski S. R., 2010, ApJ, 714, 229
Lindegren L. et al., 2018, A&A, 616, 25
LSST Dark Energy Science Collaboration, 2012, preprint (arXiv:1211.0310)
Luri X. et al., 2018, A&A, 616, 19
Majewski S. R., Skrutskie M. F., Weinberg M. D., Ostheimer J. C., 2003, ApJ, 599, 1082
Malhan K., Ibata R. A., 2017, MNRAS, 471, 1005
Malhan K., Ibata R. A., 2018, MNRAS, 477, 4063

Marigo P., Girardi L., Bressan A., Groenewegen M. A. T., Silva L., Granato G. L., 2008, A&A, 482, 883
Mateu C., Read J. I., Kawata D., 2018, MNRAS, 474, 4112
McConnachie A. W., 2012, AJ, 144, 4
Newberg H. J., Willett B. A., Yanny B., Xu Y., 2010, ApJ, 711, 32
Reid M. J. et al., 2014, ApJ, 783, 130
Robin A. C. et al., 2012, A&A, 543, A100
Sanders J. L., Bovy J., Erkal D., 2016, MNRAS, 457, 3817
Sanderson C., Curtin R., 2017, J Open Source Softw., 2, 365
Schlegel D. J., Finkbeiner D. P., Davis M., 1998, ApJ, 500, 525
Schönrich R., Binney J., Dehnen W., 2010, MNRAS, 403, 1829
Shipp N. et al., 2018, ApJ, 862, 24

This paper has been typeset from a TEX/LATEX file prepared by the author.